Title
Retinal gene therapy with a large MYO7A cDNA using adeno-associated virus

Journal
Gene Therapy, 20(8)

ISSN
0969-7128

Authors
Lopes, VS
Boye, SE
Louie, CM
et al.

Publication Date
2013-08-01

DOI
10.1038/gt.2013.3

Peer reviewed

HHS Public Access

Author manuscript

Gene Ther. Author manuscript; available in PMC 2014 February 01.

Published in final edited form as:

Gene Ther. 2013 August ; 20(8): 824–833. doi:10.1038/gt.2013.3.

Retinal gene therapy with a large *MYO7A* cDNA using adeno-associated virus

Vanda S. Lopes[1,2,*], **Shannon E. Boye**[3,*], **Carrie M. Louie**[1], **Sanford Boye**[3], **Frank Dyka**[3], **Vince Chiodo**[3], **Hugo Fofo**[2], **William W. Hauswirth**[3], and **David S. Williams**[1,#]

[1]Jules Stein Eye Institute, Departments of Ophthalmology and Neurobiology, UCLA School of Medicine, Los Angeles, CA

[2]Centre of Ophthalmology, IBILI, Faculty of Medicine, University Coimbra, PT

[3]Department of Ophthalmology, College of Medicine, University of Florida, Gainsville, FL

Abstract

Usher 1 patients are born profoundly deaf and then develop retinal degeneration. Thus they are readily identified prior to the onset of retinal degeneration, making gene therapy a viable strategy to prevent their blindness. Here, we have investigated the use of adeno-associated viruses (AAV) for the delivery of the Usher 1B gene, *MYO7A*, to retinal cells in cell culture and in *Myo7a*-null mice. *MYO7A* cDNA, under control of a *smCBA* promoter, was packaged in single AAV2 and AAV5 vectors, and as two overlapping halves in dual AAV2 vectors. The 7.9-kb *smCBA-MYO7A* exceeds the capacity of an AAV vector; packaging of such oversized constructs into single AAV vectors may involve fragmentation of the gene. Nevertheless, the AAV2 and AAV5 single vector preparations successfully transduced photoreceptor and RPE cells, resulting in functional, full-length MYO7A protein and correction of mutant phenotypes, suggesting successful homologous recombination of gene fragments. With discrete, conventional-sized dual AAV2 vectors, full-length MYO7A was detected, but the level of protein expression was variable, and only a minority of cells showed phenotype correction. Our results show that *MYO7A* therapy with AAV2 or AAV5 single vectors is efficacious, however, the dual AAV2 approach proved to be less effective.

Keywords

Usher syndrome; gene therapy; adeno-associated virus; retina; RPE; MYO7A

[#]Corresponding author: David S. Williams, Jules Stein Eye Institute, UCLA School of Medicine, 100 Stein Plaza, Los Angeles, CA 90095, dswilliams@ucla.edu.

[*]These authors contributed equally.

Conflicts of Interest

WWH and the University of Florida have a financial interest in the use of AAV therapies, and own equity in a company (AGTC Inc.) that might, in the future, commercialize some aspects of this work.

Supplementary information is available at Gene Therapy's website.

Introduction

Many inherited retinal diseases are caused by loss of function of a single gene that is expressed in the photoreceptor cells and/or the retinal pigment epithelium (RPE), with progressive retinal degeneration resulting in blindness. These diseases should therefore be preventable by the introduction of a wildtype version of the mutant gene into the photoreceptor and/or RPE cells, prior to the onset of retinal degeneration. Proof of this principle has now been demonstrated in clinical trials with patients possessing Leber congenital amaurosis, due to loss of function of the *RPE65* gene [1-4].

In Usher syndrome, retinal degeneration occurs in conjunction with deafness. In most cases, the deafness is congenital; in Usher syndrome type 1, patients are born profoundly deaf. These patients are thus readily identified when infants, prior to the onset of retinal degeneration, making gene therapy a viable strategy to prevent their blindness.

The most common form of Usher syndrome type 1 is Usher 1B, which accounts for at least half of Usher 1 cases. It is caused by mutations in the *MYO7A* gene [5]. Together with light chains, MYO7A forms the actin-based motor, myosin 7a. Myosin 7a has a variety of functions in the photoreceptor and RPE cells [6-11]. The recessive inheritance of Usher syndrome, together with *MYO7A* disease alleles that are likely null, indicate that Usher 1B is primarily due to loss of MYO7A function e.g. [12], so that the progressive blindness should therefore be preventable by delivering a wildtype gene to the photoreceptor and RPE cells prior to any cell degeneration. A limitation is that *MYO7A* is a large gene; its cDNA is nearly 7 kb [13, 14]. This large size is particularly a concern for using adeno-associated virus (AAV) to deliver the gene. AAV has been used successfully in clinical and preclinical retinal gene therapy experiments [1-4, 15], but its nominal packaging size was reported to be ~5.3 kb [16]. Because of the size of *MYO7A*, we initially studied the use of a lentiviral vector to deliver *MYO7A* cDNA to the RPE and photoreceptor cells [17]. Following subretinal injection of mice, we observed correction of mutant phenotypes in the RPE and photoreceptor cells. However, the integrating nature of lentiviral vectors poses a concern with respect to the introduction of insertional mutagenesis, as well as different responses among different cells due to cell to cell variation in the integration of the gene. By contrast, AAV transduction results in mostly episomal DNA, which has been shown to be stable in terminally-differentiated cells, such as photoreceptor and RPE cells [18, 19].

More recently, we showed that AAV5 was able to mediate expression of full length MYO7A protein in RPE cells in primary culture [20]. Subsequent studies by three independent groups found that AAV could deliver other large genes, although they showed that the DNA was first fragmented into sizes consistent with canonical AAV packaging (i.e. less than 5 kb), and then the fragmented genes reassemble after delivery to the cell, presumably by recombination, to yield a full length cDNA [21-23]. The ability of different cells to reassemble a given gene is likely to vary. In the present study, we have tested the ability of AAV-*MYO7A* to transduce RPE and photoreceptor cells *in vivo*, and to correct mutant phenotypes in mice that are null for the Usher 1B orthologue, *Myo7a*. We demonstrate efficacy not only with AAV5, but also the more commonly used serotype, AAV2.

Due to the possible heterogeneous nature of genes delivered by these single AAV vectors, we also tested a dual vector preparation, with two AAV2 vectors, each containing an overlapping half of *MYO7A*. Comparable dual vector systems have been tested previously, showing some modest success as gene therapy vectors in animal models of Duchenne's muscular dystrophy [24, 25], but, to date, no such approach has been used to address retinal disease associated with a large gene. Our results indicate that this dual vector approach is significantly less effective than using the single AAV2 or AAV5 vectors to deliver functional MYO7A to the photoreceptor and RPE cells.

RESULTS

AAV-MYO7A single vector preparations

AAV vector plasmid was engineered to contain a truncated chimeric *CMV*/chicken β-actin promoter, sm*CBA* [26] and the 6.7-kb cDNA encoding the full length isoform 2 of human MYO7A (Fig. 1a). The sm*CBA* promoter exhibits the same tropism and activity in mouse retinas as that of the full-length *CBA* promoter [26, 27]. Titers of 10^{12} to 10^{13} particles/mL were obtained for different lots of AAV2-*MYO7A* and AAV5-*MYO7A*. A concentration of 10^{12} particles/mL was regarded as our standard concentration (1x), from which dilutions were made. The experiments were performed with virus obtained from three separate preparations. No differences in expression or phenotype correction, as described below, were observed among the different lots for AAV2-*MYO7A* or AAV5-*MYO7A* at a given concentration.

MYO7A expression in cell culture

Transduction of primary cultures of *Myo7a*-null RPE cells with 1x single AAV2-*MYO7A* or AAV5-*MYO7A* resulted in the expression of a polypeptide that, by western blot analysis, had an apparent mass that was comparable to that of WT MYO7A protein, and was present at similar levels to that found in primary cultures of *Myo7a*$^{+/-}$RPE cells (Fig. 1b). Likewise, a single band of appropriate size was detected on western blots of HEK293A cells (data not shown). Immunofluorescence of the primary RPE cells showed that the MYO7A protein, resulting from 1x single AAV-*MYO7A* treatment of MYO7A-null cells, had a subcellular localization pattern that was comparable to that of endogenous MYO7A in control cells, indicating the generation of appropriately targeted protein (Fig. 1c-f). ARPE19 cells were also infected with 1x or diluted (1:100) AAV2-*MYO7A* or AAV5-*MYO7A*, and compared with non-treated cells. An increase in MYO7A immunofluorescence was detected in the treated cells, and the intracellular localization of the label was comparable to that in untreated cells (Suppl. Fig. 1a-e).

Localization of MYO7A *in vivo*

Most retinal MYO7A is found in the RPE [28], however, the protein is also present in the connecting cilium and pericilium of the photoreceptor cells [29, 30]. A diagram illustrating this distribution and the retinal functions of MYO7A has been published in a recent review [11].

Three weeks following injection of 1x AAV2-*MYO7A* or AAV5-*MYO7A* into the subretinal space of *Myo7a*-null mice, retinal tissue was examined by immunoelectron microscopy to

test for MYO7A expression. Near the site of injection (within 1.4 mm), immunogold label was evident in the photoreceptor cells, where it was localized in the connecting cilium and pericilium, comparable to that in WT retinas (Fig. 2a-e). Label was also present throughout the RPE cells, particularly in the apical cell body region (Fig. 2f-g), as found in WT retinas [9, 29]. At the periphery of the retina, no significant immunolabel was detected (Suppl. Fig. 2).

MYO7A has a similar distribution in both rod and cone photoreceptor cells [7]. To test whether treatment with AAV-*MYO7A* also affected cone photoreceptor cells, we determined whether MYO7A was also present in the ciliary region of cone photoreceptors. We performed double immunoEM of treated retinas, using a MYO7A antibody together with an antibody specific for rod opsin. Although there are only a small number of cones with aligned connecting cilia found in each ultrathin section, MYO7A immunogold label was evident in the connecting cilium and periciliary region of these cones, which were identified by lack of rod opsin labeling in their outer segments (in contrast to the surrounding rod outer segments) (Fig. 2h, i). Hence, AAV2-*MYO7A* and AAV5-*MYO7A* can transduce cone as well as rod photoreceptor cells.

Dose-dependent MYO7A expression in photoreceptor and RPE cells

To determine the levels of MYO7A expression following treatment with different concentrations of AAV2-*MYO7A* and AAV5-*MYO7A* (1x, 1:10 or 1:100 dilutions), we quantified MYO7A immunogold labeling in EM images, taken within 1.4 mm of the injection site. Reliable detection of MYO7A in the photoreceptor cells, where its distribution is limited to the connecting cilium and pericilium, requires the higher resolution provided by electron microscopy [29]. Immunogold particle density was measured in images of the photoreceptor connecting cilium and pericilium, shown in complete longitudinal section (from the basal bodies to the base of the outer segment), and in images showing the RPE cells in apical to basal section. Particle density was expressed as particles per length of cilium for the photoreceptor cells (each connecting cilium is ~1.2 um long), and as particles per area for the RPE cells (the entire area between the apical and basal surfaces was included). Particle density is dependent on exposure of epitopes on the surface of the section, and, as such, provides a relative linear measure of antigen density under the conditions used here (i.e. grids were etched and labeled in an identical manner, and the labeling was not so dense as to be affected by steric hindrance).

Treatment with 1x AAV2-*MYO7A* or AAV5-*MYO7A* resulted in 2.5-2.7 times the density of immunolabel in the photoreceptor cilium, compared with that found in WT retinas, while the 1:10 and 1:100 dilutions resulted in a density of immunolabel that was more comparable to WT levels (Fig. 2j and l; Suppl. Fig. 3). Quantification of immunogold label in the RPE showed that injection of AAV2-*MYO7A* resulted in 2.7 times more label than in WT, with the 1:10 and 1:100 dilutions showing no significant difference (Fig. 2k). In contrast, the level of MYO7A immunolabel in the RPE of retinas injected with AAV5-*MYO7A* varied in relation to virus titer, with the full dose virus effecting 2.2-fold more MYO7A than that found in WT RPE, the 1:10 dilution effecting WT levels, and the 1:100 dilution resulting, on average, ~60% of WT levels (Fig. 2m).

These counts of labeling density indicate that 1x AAV-*MYO7A* resulted in more than double the normal level of MYO7A expression in both the photoreceptor and RPE cells. The distribution of MYO7A was not affected by this overexpression in the photoreceptor cells. In the RPE cells, the overall distribution of MYO7A was comparable to WT, with a higher concentration in the apical cell body region. However, with 1x AAV2-*MYO7A* or 1x AAV5-*MYO7A*, the proportion of MYO7A that was associated with melanosomes was only just over half that in WT RPE: in WT RPE, we found that 42% of the MYO7A immunogold particles were located near the membrane of melanosomes; in retinas treated with 1X AAV2-MYO7A, we found 23%; and in retinas treated with 1X AAV2-MYO7A, we found 24%. This difference is possibly because the proteins that link MYO7A to the melanosomes, MYRIP and RAB27A [31, 32], may have remained near WT levels, and thus limited the absolute amount of MYO7A that could associate with the melanosomes.

Despite the overexpression of MYO7A, no pathology was evident in retinas, up to 3 months after injection of 1x (or 1:10) AAV2-*MYO7A*. However, two out of six retinas injected with 10^{13} particles/mL of AAV5-*MYO7A* (i.e. 10x) showed evidence of photoreceptor cell loss across the retina after 3 weeks (AAV2-*MYO7A* was not tested at this titer) (Suppl. Fig. 4).

Correction of melanosome localization in the RPE

In *Myo7a*-mutant mice, melanosomes are absent from the apical processes of the RPE cells [6]. This mutant phenotype is evident at all neonatal ages, and is due to loss of actin-based transport of the melanosomes by the myosin 7a motor [9]. Three weeks following injection of 1x AAV2-*MYO7A* or AAV5-*MYO7A* into the subretinal space of *Myo7a*-null mice, melanosomes were observed to have a normal distribution in all RPE cells near the site of injection (within 1.4 mm) (n=10 each for AAV2-*MYO7A* and AAV5-*MYO7A*) (Fig. 3a-c). Well away from the injection site, a mixture of corrected and uncorrected RPE cells was evident, while, at the periphery of the retina, the cells all exhibited the *Myo7a*-mutant phenotype, indicating lack of correction in this region (Fig. 3d-f). The correction of melanosomes was still evident in retinas that were fixed 3 months after injection (Suppl. Fig. 5). Correction was also observed in all eyes injected with 1:10 dilution AAV2-*MYO7A* (n=6) or AAV5-*MYO7A*(n=6), as well as in all eyes injected with 1:100 dilution AAV2-*MYO7A* (n=6) or AAV5-*MYO7A* (n=6), although with the 1:100 dilution some of the RPE cells near the site of injection were not corrected.

Correction of opsin distribution

Myo7a-mutant mice have an abnormal accumulation of opsin in the connecting cilia of the photoreceptor cells, a phenotype that is evident by immunoEM with opsin antibodies [7]. This mutant phenotype suggest that myosin 7a functions in the vectorial delivery of opsin to the outer segment [7]. Quantification of immunogold opsin labeling in the connecting cilia, demonstrated that this phenotype was corrected with 1x AAV2-*MYO7A* or AAV5-*MYO7A* (Fig. 3g; Suppl. Fig. 6). This analysis also showed phenotype correction with 1:100 dilutions, although the data indicated that a full WT phenotype was not achieved (Fig. 3g), despite WT levels of MYO7A (Fig. 2j, l), suggesting that some of the MYO7A may not be fully functional.

AAV2-*MYO7A* dual vector preparations

The preceding results demonstrate that a single AAV vector is capable of delivering functional *MYO7A* to the RPE and photoreceptor cells *in vivo*. Because the size of smCBA-MYO7A is ~2 kb larger than the nominal carrying capacity of an AAV [16], this transduction might involve undefined fragmentation of the sm*CBA-MYO7A* cDNA, followed by reassembly of plus and minus cDNA strands after delivery to the cell, as shown for other large genes [21-23]. To evaluate whether two AAV vectors containing defined, overlapping fragments of *MYO7A* cDNA (1365 bases) were also capable of mediating full length MYO7A expression, we developed an AAV2-based dual vector system (Fig. 4a). Two separate lots of the AAV2-*MYO7A*(dual vector) were prepared, each containing equal concentrations of AAV2-sm*CBA-MYO7A*(5′-half) and AAV2-*MYO7A*(3′-half). The titer of the first lot contained 2.5×10^{12} particles/mL of each vector, and the second lot contained 4×10^{12} particles/mL.

MYO7A expression with AAV2 dual vectors

Western blot analysis of primary cultures of *Myo7a*-null RPE cells, infected with AAV2-*MYO7A*(dual vector) of either lot, showed that the cells expressed a MYO7A-immunolabeled polypeptide of comparable mass to that of WT MYO7A (Fig. 4b). However, the overall expression level of MYO7A in the treated *Myo7a*-null RPE cells was significantly less than that found in primary cultures of *Myo7a*$^{+/-}$ RPE cells (Fig. 4b), and significantly less than that expressed after infection by the single AAV2 or AAV5 vectors (Fig. 4c). Quantitative analysis of western blots showed that *Myo7a*-null RPE cells, transduced with the single vectors (1x), AAV2-MYO7A or AAV5-MYO7A, or with AAV2-MYO7A(dual vector), expressed MYO7A at levels that were 82%, 111%, and 10%, respectively, of the level of MYO7A in *Myo7a*$^{+/-}$ RPE cells.

Immunofluorescence of primary *Myo7a*-null RPE cells, infected with AAV2-*MYO7A*(dual vector), showed that a few cells scattered throughout the culture exhibited very high levels of MYO7A, but all other cells contained insignificant levels (Fig. 4d-f). The cells overexpressing MYO7A typically had altered morphology, suggesting that the high levels of MYO7A may be toxic. Similarly, immunofluorescence of ARPE19 cells, infected with AAV2-*MYO7A*(dual vector), resulted in a minority of cells that were labeled intensely with MYO7A antibody, with most of the cells appearing to express only endogenous levels of MYO7A (Fig. 4g; Suppl. Fig. 1f).

Immunolabeling of retinas, prepared 3 weeks after subretinal injection with AAV2-*MYO7A*(dual vector) of either lot, also showed only a few RPE cells and photoreceptor cells with clear MYO7A expression, although significant overexpression was not evident in this *in vivo* experiment. Immunogold particle counts from images of ultrathin sections were used to quantify the level of MYO7A expression in *Myo7a*-null retinas that were treated with the second lot of AAV2-*MYO7A*(dual vector). Within 1.4 mm of the injection site, MYO7A immunolabeling of the connecting cilium and pericilium of the photoreceptor cells was a mean of 48% of that in WT retinas: 2.8 particles/μm (n=3 retinas) compared with 6.5 particles/μm for WT (n=3 retinas). The mean label density in apical-basal sections of the RPE was 35% of that in WT retinas: 11 particles/100 μm^2 compared with 31 particles/100

μm^2 for WT. However, it was clear that these lower means were achieved by some cells expressing near normal amounts of MYO7A and the majority expressing very little; over half the cells had fewer than 10 particles/100 μm^2 (Fig. 4h).

Correction of *Myo7a*-mutant phenotypes with AAV2 dual vectors

Eyes were analyzed for correction of melanosome localization and ciliary opsin distribution within 1.4 mm of the injection site. With either lot of AAV2-*MYO7A*(dual vector), some RPE cells (29% for lot 1 treatment (n=6 retinas), 35% for lot 2 treatment (n=9 retinas)) were observed to have a normal apical melanosome distribution, but most of the cells in this region retained the *Myo7a*-mutant phenotype, resulting in a mosaic effect (Fig. 5a) that contained a much lower proportion of corrected cells than that observed with a 1:100 dilution of either of the single vectors. The only correction observed in 3 eyes injected with a 1:10 dilution of AAV2-*MYO7A*(dual vector) (first lot), was in 18% of the RPE cells in one of the retinas. With full-strength of AAV2-*MYO7A*(dual vector) (second lot), opsin immunogold density averaged 3.2 + 0.4 particles/μm of cilium length, which was reduced from untreated retinas (4.2 + 0.8 particles/μm; p=0.003), but still greater than WT levels (1.1 + 0.2 particles/μm), suggesting that most cells were not corrected. An example of a corrected cell is shown in Fig. 5g.

Using immunoelectron microscopy, we tested for a correlation between phenotype correction and the expression level of MYO7A, determined by the mean concentration of immunogold particles in an apical-basal section of each RPE cell (Fig. 5b-e). From the eyes injected with AAV2-*MYO7A*(dual vector) (second lot), we found that the corrected RPE cells contained a mean of 108% of the WT level of MYO7A (the minimum level was 82%). RPE cells that were not corrected contained a mean of 26% of the WT level of MYO7A (the maximum level was 92%). While these data show that higher expression of MYO7A is correlated with phenotype correction (Fig. 5f), it also indicates that some of the labeled MYO7A protein is not functional, given that melanosomes are localized normally in mice that are heterozygous for the *Myo7a*-null allele and have only ~50% of the WT level of MYO7A.

DISCUSSION

The efficacy of AAV2- and AAV5-mediated *MYO7A* delivery to the retinas of *Myo7a*-mutant mice was tested in a preclinical study aimed at developing a treatment for preventing blindness in Usher 1B. Despite the large size of sm*CBA-MYO7A* relative to the carrying capacity of AAV, single vector preparations of either serotype effected MYO7A expression in RPE and photoreceptor cells and corrected the mutant phenotypes in both cell types. In a different approach, using two discrete AAV2 vectors, each containing a different half of *MYO7A* cDNA, with a central overlapping region, MYO7A expression was detected, but only in a minority of cells, both in culture and *in vivo*. Likewise, the correction of mutant phenotypes was sporadic. These findings demonstrate the therapeutic potential of using a single AAV vector to deliver *MYO7A*, but they indicate limitations with an overlapping dual AAV vector approach.

MYO7A delivery by AAV2 and AAV5 single vectors

Demonstration that AAV vectors mediate safe and effective therapy in clinical trials [1-4, 15] has been limited to the delivery of small genes or reduced versions of larger ones. Recombinant DNA can only be efficiently packaged into AAV if the total DNA is less than about 5.3 kb. Capsids containing DNA larger than 5.3 kb exhibit a progressively reduced transduction efficiency until reaching the physical encapsidation limit of ~6 KB [16]. The strategy of creating "mini" proteins, reduced to minimally essential domains, has been used in an attempt to make gene therapy with AAV tractable for large genes, such as dystrophin [33], although, limitations of this approach have been reported recently [15, 25]. However, the mini gene approach is of little use for large molecular motor genes, such as *MYO7A*. MYO7A is composed of essential motor, neck and tail domains, which provide the mechanoenzymatic properties, a lever for the step-wise motion, and cargo binding sites, respectively. The essential nature of each domain is clear from structure-function studies of myosins [34-36]. Moreover, *MYO7A* mutations throughout the gene have been shown to cause Usher 1B, demonstrating that a perturbation of any major domain is pathogenic e.g. [12] (http://www.hgmd.cf.ac.uk/ac/gene.php?gene=MYO7A).

Previously, we showed that a single AAV5 vector was able to deliver *MYO7A* and *ABCA4* (8.9 kb) cDNA, resulting in full-length protein expression in cell culture [20]. *In vivo* studies with *Abca4*-mutant mice indicated ABCA4 expression and a reduction in the abnormally-high levels of lipofuscin in the RPE that results from ABCA4 dysfunction. More recently, it has been shown that full-length, large gene reconstruction results from recombination between fragmented plus and minus cDNA strands packaged into separate capsids [21-23]. Using single-molecule sequencing, Kapranov et al. found that the accommodation of large genomes by AAV involves encapsidation of only the 3′ ITR and cleavage at the 5′ end, resulting in a heterogeneous population of fragmented genomes [37]. These fragments thus require a recombination event between appropriate overlapping genome fragments to reconstitute a full-length cDNA in cells containing multiple viral copies.

Our results show that transduction of photoreceptor and RPE cells with either the AAV2 or AAV5 single vectors results in the expression of MYO7A of the correct molecular mass. If fragmentation of the gene is occuring during packaging into the vectors, these results indicate that the fragments recombine successfully within the target cells. The extent of recombination may be dependent on the recombinogenic nature of the transgene itself; *MYO7A*, in the present study, seems to recombine well from the fragments, whereas dystrophin, for example, recombines relatively poorly [22].

The level of expression of MYO7A observed *in vivo* was related to the titer of the vector delivered, with the exception of MYO7A levels in the RPE following treatment with AAV2-*MYO7A*; these levels were similar across a 100-fold dilution range. Even with this exception, the relative expression between the photoreceptor and RPE cells did not vary substantially from the ratio found in WT retinas, despite the use of a non-native promoter in the vector, the large difference in MYO7A levels between the photoreceptor and RPE cells, and the use of two different AAV serotypes.

Overexpression of MYO7A has been shown to be toxic in a previous study, using lentiviral delivery of *MYO7A* under a full CMV promoter [17], and, in the present study, we observed extensive photoreceptor cell death, following subretinal injection of 10^{13} vector genome containing particles/mL of AAV5-*MYO7A* (i.e. 10x). Nevertheless, the present results indicate that there is a fairly large tolerance for excessive MYO7A levels. Phenotype correction with no indication of deleterious effects was observed over a wide range of vector titers (10^{10} to 10^{12} particles/mL), resulting in a wide range of MYO7A levels, up to nearly 3 times that found in the photoreceptor and RPE cells of WT retinas. Some overexpression may to be necessary in the photoreceptor cells, where some of the MYO7A was suggested to be not fully functional, based on counts of MYO7A and opsin immunogold particles, and the degree of correction of the opsin distribution.

MYO7A delivery by AAV2 dual vector

We also investigated whether a dual vector system composed of two vectors containing specfic overlapping *MYO7A* cDNA fragments would also promote therapy. AAV2 dual vectors were packaged so that each contained a 3′ or 5′ segment of the cDNA that was less than 5 kb, and each part shared an overlapping region of 1365 bases. Western blot analysis showed that infected cells were able to generate full length MYO7A from the two parts, however, immunolabeling of cells *in vitro* and *in vivo* showed that the majority of cells failed to make significant amounts of the protein. Moreover, the RPE cells in culture that did contain MYO7A expressed it at excessive levels, and our data correlating MYO7A immunolabeling with phenotype correction in the RPE suggested that some of the MYO7A that was produced *in vivo* was not functional. Further studies are needed to investigate the nature of this non-functional protein, as well as that which may have been generated by the photoreceptors following infection with single vector AAV-*MYO7A*.

The failure of the majority of the cells to express any detectable MYO7A seems to be independent of the efficiency of vector delivery to the target cells. The titers of the dual AAV2 vectors were slightly higher than the 1x titer used for the single AAV2 vector, yet the single vector was efficacious, resulting in WT levels of MYO7A, even at a 1:100 dilution. The probability of the two halves of *MYO7A* cDNA recombining therefore appears to be very low in most of the RPE and photoreceptor cells.

Can the dual vector design be improved so that it could be used for Usher 1B retinal gene therapy? Different overlapping regions of the gene may offer more reliable homologous recombination, although the choice of regions is quite limited for *MYO7A*, since neither half can be made much larger without exceeding the vector packaging limit. Previous studies have compared transduction with a single vector and dual overlapping vectors, and showed that transduction is typically less efficient with the dual vector, although they have only tested genes that are less than 5 kb [38, 39]. An alternative is to use dual vectors in which the two segments of the cDNA are designed to trans-splice together. An earlier report showed an order of magnitude improvement with this design compared with homologous recombination via a simple overlapping region, although it still fell short of transduction with a single vector [40]. Combining trans-splicing with recombination of an overlapping region has yielded more promising results [41], and could be applied to *MYO7A*. However,

when such hybrid (transplicing + overlapping) vectors were directly compared to an overlapping only dual vector system *in-vivo*, the overlapping vector proved to be most efficient [25].

An alternative approach for increasing the efficiency of a dual vector system may be the use of a different AAV serotype. The decision to test AAV2 in the present study was based on the current clinical use of this serotype [1-4, 15]. Other serotypes, such as AAV5 and AAV8, have been reported to transduce photoreceptor and RPE cells with greater efficiency 42, 43, although, in the present study, the AAV5-*MYO7A* single vector was not found to transduce these cells with any greater efficiency than the AAV2-*MYO7A* single vector (Fig. 2). AAV vectors containing single or multiple tyrosine to phenylalanine (Y-F) mutations on their capsid surface have been found to increase transduction efficiency and expression kinetics relative to unmodified vectors, possibly due to the ability of the virus to avoid proteosomal degradation [44]. The increased capacity of an AAV8(Y-F) mutant to restore function and preserve structure has been shown in two other mouse models of retinal disease [45, 46]. However, in the case of *MYO7A* therapy, a concern is that approaches that increase the general level of expression of MYO7A protein might also to result in pathology of the higher expressing cells, as already indicated by the cultured RPE cells that were treated with the dual vector in the present study.

Potential treatment for Usher 1B

The mouse model we have used in the present study contains a null mutation for *Myo7a* [7, 47]. Like other *Myo7a*-mutant mice, and indeed most other Usher 1 mouse models, their retinas do not degenerate [30, 47]. Nevertheless, the mouse represents a useful model for testing the efficacy of retinal gene therapy for Usher 1B. First, MYO7A has been demonstrated to function in the motility of melanosomes of human RPE cells, as it does in mouse RPE cells [48]. Second, although null *MYO7A* alleles seem to have less severe retinal disease among Usher 1B patients, the primary effect of *MYO7A* mutations is loss of function of the mechanoenzyme [12]. Therefore, testing the correction of mutant phenotypes in a *Myo7a*-null mouse, as an indicator of appropriate expression of functional MYO7A in the retina, is a valid preclinical approach for identifying a treatment to prevent blindness in Ush1B patients.

In the present study, we have shown that single AAV2 or AAV5 vector delivery of *MYO7A* to the photoreceptor and RPE cells provides effective therapy. Although this approach likely includes the production of random fragments of *MYO7A*, these fragments successfully recombined to express functional MYO7A, resulting in correction of mutant phenotypes. In contrast, recombination of two defined overlapping fragments of *MYO7A*, delivered by dual AAV2 vectors, was found to be inconsistent, with only sporadic phenotype correction observed.

Materials and Methods

Animals

Shaker1 mice carrying the 4626SB allele, an effective null mutation [7, 47], were used on the C57BL6 genetic background, and maintained and genotyped as described [7, 8]. They were maintained on a 12-hr light/12-hr dark cycle, with exposure to 10-50 lux of fluorescent lighting during the light phase, and were treated according to NIH and UCLA animal care guidelines. Homozygous mutants were distinguished from the heterozygous controls by their hyperactivity, head-tossing and circling behavior [49], and/or by a PCR/restriction digest assay.

Construction of AAV Vectors

Single vector platform: AAV vector plasmid, containing the truncated chimeric CMV/chicken β-actin promoter (sm*CBA*) [26] and *MYO7A* cDNA, was constructed by removing the full *MYO7A* cDNA from pEGFP-C2 by EagI and Sal I digest and ligating into pTR-smCBA-GFP digested with Not I and Sal I (to remove GFP). The *MYO7A* cDNA (6.7 kb) corresponds to isoform 2 of human *MYO7A*, and was the same as that used previously [17], which was based on the sequence published by Chen et al. [13]. *MYO7A* isoform 2 is 114-kb shorter than isoform 1 [13, 14]. The *MYO7A* cDNA and resulting junctions were fully sequenced prior to packaging. Vector plasmid was packaged and titered in AAV2 and AAV5 according to previously published methods [50, 51]. Titers of 10^{12} to 10^{13} particles/mL were obtained for different batches of AAV2-*MYO7A* and AAV5-*MYO7A.*

Dual vector platform: Two separate vector plasmids were constructed. Vector A contains the strong, ubiquitous "sm*CBA*" promoter and *MYO7A* cDNA encoding the N-terminal portion. Vector B contains *MYO7A* cDNA encoding the C-terminal portion and a poly-A signal sequence. Each vector plasmid contains both inverted terminal repeats (ITRs). Using PCR with full length cDNA of *MYO7A* isoform 2 (NCBI # NM_001127180) as template, the *MYO7A* cDNA was divided roughly in half with amplicons encompassing nucleotide positions 1 through 3644 (Vector A) and 2279 through 6647 (Vector B) relative to ATG start position 1 . The resulting two vector plasmids share 1365 bp of overlapping *MYO7A* sequence and are 5.0 and 4.9 KB in length, respectively, well within the size limitation of a standard AAV vector. Both vector plasmids were sequence verified and separately packaged by standard AAV production methods [50, 51]. The titer of the first lot contained 2.5×10^{12} particles/mL of each vector, and the second lot contained 4×10^{12}particles/mL of each vector.

Viral delivery *in vitro*

HEK293A cells (Invitrogen, CA, USA), grown in DMEM with 10% FBS and 1x NEAA and Pen/Strep (Invitrogen, CA, USA) were plated in 6 well-plates. The next day cells were incubated, at 37 °C and 5% CO_2, with AAV2- and AAV5-MYO7A at an MOI of 10,000 viral particles/cell in 500 μl of complete medium, containing also 40 μM of calpain inhibitor (Roche). Two hours later complete medium was added. The next day the medium was changed, and cells were incubated for an additional 48 hrs. Alternatively, some cells were

transfected with 1 μg of vector pTR-sm*CBA-MYO7A*, complexed with Lipofectamine 2000 (ratio 1:3), according to the manufacturer's instructions (Invitrogen, CA, USA).

Primary mouse RPE cells were derived from P14-P16 *Myo7a*-null animals and cultured in 24-well dishes, as described [8, 52]. After 48 hrs in culture, cells were transduced with viruses. Cells were incubated in 100 μl of complete medium, containing 40 μM of calpain inhibitor and 10,000 viral particles/cell from the full-strength AAV stocks. After 2 hours, 400 μl of complete medium was added to each well, and incubated overnight. The medium was changed the following day, and cells were incubated for an additional 48 hrs.

ARPE19 cells (ATCC) were cultivated in DMEM/F-12 with 10% FBS and split into 24-well plates with glass coverslips. Cells were grown to confluency and then transduced in the same way as were the primary RPE cells.

MYO7A expression analysis by Western blot and Immunofluorescence

HEK293A and primary mouse RPE cells that were tranduced with AAV-*MYO7A* were collected 3 days post-transduction. For western blot analyses, cells were collected and lysed in 20 mM TRIS, pH 7.4, 5 mM MgCl2, 10 mM NaCl, 1 mM DTT and 1x protease inhibitor cocktail (Sigma, MO, USA). Equivalent amounts of total protein were separated on a 7.5 % SDS-PAGE gel. After transfer, blots were blocked with 5% non-fat milk, and probed with mouse anti-MYO7A antibody, generated against residues 927-1203 of human MYO7A (Developmental Studies Hybridoma Bank, Iowa, USA) [53], and mouse anti-actin antibody (Sigma, MO, USA) as a loading control.

Immunofluorescence was performed with ARPE19 and mouse RPE primary cells, 3 days after infection. Cells were fixed in 4% formaldehyde, blocked with blocking solution (0.5% BSA/0.05% saponin in PBS), incubated with the mouse anti-MYO7A followed by goat anti-mouse Alexa-568 (Molecular Probes, Invitrogen, USA). Coverslips were mounted with mounting medium containing DAPI (Fluorogel II, Electron Microscopy Sciences, USA) and visualised on a Leica confocal system.

Viral Delivery *in vivo*

Mice were anesthetized with 2.0-3.0% isoflurane inhalation. The pupils of the animals were dilated with 1% (w/v) atropine sulfate and 2.5% phenylephrine. A local anaesthetic, 0.5% proparacaine hydrochloride, was also administered. A sclerotomy in the temporal limbus was performed with a 27G needle. A 32 gauge blunt needle, attached to a microsyringe pump (WPI, USA), was inserted and 1 μl of viral solution was injected into the ventral subretinal space of P14-P16 animals. Retinal detachment was visualised under a dissecting microscope, and registered as indication of a positive subretinal injection.

Light Microscopy and Immunoelectron Microscopy of Retinas

Eyecups were processed for embedment in either LR White or Epon, and semithin and ultrathin sections were prepared. Semithin sections were stained with toluidine blue and visualised on a Leica confocal system. Ultrathin sections were labeled with purified MYO7A pAb 2.2 [29] and monoclonal anti-opsin (1D4, R. Molday), followed by gold-

conjugated secondary antibodies (Electron Microscopy Sciences, USA), as described previously [10]. Negative control sections processed at the same time included those from *Myo7a*-null retinas, and, as positive control, WT animals were used.

MYO7A immunogold density was determined on sections of age-matched WT, *Myo7a*-null retinas and retinas of *Myo7a*-null animals that had been injected with AAV-*MYO7A* at P14-16 and dissected three weeks later. For quantification of the immunolabel all the gold particles in a complete section of each RPE cell were counted. The area of each cell's profile was determined using ImageJ software. For background labeling, the concentration of label in sections of untreated *Myo7a*-null animals was measured. Data are expressed with this background labeling subtracted.

The concentration of MYO7A and opsin immunogold labeling in the connecting cilia of photoreceptor cells was determined by counting gold particles along longitudinal profiles of connecting cilia and measuring the length of each profile.

Analysis and quantifications were performed in a minimum of 3 different retinas, from three different animals. Statistical analysis was performed using one tail Student t-test.

Supplementary Material

Refer to Web version on PubMed Central for supplementary material.

Acknowledgments

We thank Nuno Martins for technical assistance. The study was supported by grants from the Foundation Fighting Blindness, the Macula Vision Research Foundation, Research to Prevent Blindness (RPB), and the NIH (EY07042 to DSW, core grant EY00331, and EY021721 to WWH). CML was supported by NIH training grant GM008243. HF was supported by an FCT PhD fellowship. DSW is a Jules and Doris Stein RPB Professor.

References

1. Bainbridge JW, Smith AJ, Barker SS, Robbie S, Henderson R, Balaggan K, et al. Effect of gene therapy on visual function in Leber's congenital amaurosis. N Engl J Med. 2008; 358:2231–9. [PubMed: 18441371]
2. Maguire AM, Simonelli F, Pierce EA, Pugh EN Jr. Mingozzi F, Bennicelli J, et al. Safety and efficacy of gene transfer for Leber's congenital amaurosis. N Engl J Med. 2008; 358:2240–8. [PubMed: 18441370]
3. Hauswirth WW, Aleman TS, Kaushal S, Cideciyan AV, Schwartz SB, Wang L, et al. Treatment of leber congenital amaurosis due to RPE65 mutations by ocular subretinal injection of adeno-associated virus gene vector: short-term results of a phase I trial. Human gene therapy. 2008; 19:979–90. [PubMed: 18774912]
4. Cideciyan AV, Aleman TS, Boye SL, Schwartz SB, Kaushal S, Roman AJ, et al. Human gene therapy for RPE65 isomerase deficiency activates the retinoid cycle of vision but with slow rod kinetics. Proc Natl Acad Sci U S A. 2008; 105:15112–7. [PubMed: 18809924]
5. Weil D, Blanchard S, Kaplan J, Guilford P, Gibson F, Walsh J, et al. Defective myosin VIIA gene responsible for Usher syndrome type 1B. Nature. 1995; 374:60–61. [PubMed: 7870171]
6. Liu X, Ondek B, Williams DS. Mutant myosin VIIa causes defective melanosome distribution in the RPE of shaker-1 mice. Nat Genet. 1998; 19:117–118. [PubMed: 9620764]
7. Liu X, Udovichenko IP, Brown SDM, Steel KP, Williams DS. Myosin VIIa participates in opsin transport through the photoreceptor cilium. J Neurosci. 1999; 19:6267–6274. [PubMed: 10414956]

8. Gibbs D, Kitamoto J, Williams DS. Abnormal phagocytosis by retinal pigmented epithelium that lacks myosin VIIa, the Usher syndrome 1B protein. Proc Natl Acad Sci U S A. 2003; 100:6481–6486. [PubMed: 12743369]
9. Gibbs D, Azarian SM, Lillo C, Kitamoto J, Klomp AE, Steel KP, et al. Role of myosin VIIa and Rab27a in the motility and localization of RPE melanosomes. J Cell Sci. 2004; 117:6473–83. [PubMed: 15572405]
10. Lopes VS, Gibbs D, Libby RT, Aleman TS, Welch DL, Lillo C, et al. The Usher 1B protein, MYO7A, is required for normal localization and function of the visual retinoid cycle enzyme, RPE65. Hum Mol Genet. 2011
11. Williams DS, Lopes VS. The many different cellular functions of MYO7A in the retina. Biochem Soc Trans. 2011; 39:1207–10. [PubMed: 21936790]
12. Jacobson SG, Cideciyan AV, Gibbs D, Sumaroka A, Roman AJ, Aleman TS, et al. Retinal Disease Course in Usher Syndrome 1B due to MYO7A Mutations. Investigative ophthalmology & visual science. 2011
13. Chen ZY, Hasson T, Kelley PM, Schwender BJ, Schwartz MF, Ramakrishnan M, et al. Molecular cloning and domain structure of human myosin-VIIa, the gene product defective in Usher syndrome 1B. Genomics. 1996; 36:440–448. [PubMed: 8884267]
14. Weil D, Levy G, Sahly I, Levi-Acobas F, Blanchard S, El-Amraoui A, et al. Human myosin VIIA responsible for the Usher 1B syndrome: a predicted membrane-associated motor protein expressed in developing sensory epithelia. Proc Natl Acad Sci U S A. 1996; 93:3232–3237. [PubMed: 8622919]
15. Bowles DE, McPhee SW, Li C, Gray SJ, Samulski JJ, Camp AS, et al. Phas. 1 Gene Therapy for Duchenne Muscular Dystrophy Using a Translational Optimized AAV Vector. Molecular therapy : the journal of the American Society of Gene Therapy. 2012; 20:443–55. [PubMed: 22068425]
16. Grieger JC, Samulski RJ. Packaging capacity of adeno-associated virus serotypes: impact of larger genomes on infectivity and postentry steps. J Virol. 2005; 79:9933–44. [PubMed: 16014954]
17. Hashimoto T, Gibbs D, Lillo C, Azarian SM, Legacki E, Zhang XM, et al. Lentiviral gene replacement therapy of retinas in a mouse model for Usher syndrome type 1B. Gene therapy. 2007; 14:584–94. [PubMed: 17268537]
18. Yang GS, Schmidt M, Yan Z, Lindbloom JD, Harding TC, Donahue BA, et al. Virus-mediated transduction of murine retina with adeno-associated virus: effects of viral capsid and genome size. Journal of virology. 2002; 76:7651–60. [PubMed: 12097579]
19. Acland GM, Aguirre GD, Bennett J, Aleman TS, Cideciyan AV, Bennicelli J, et al. Long-Term Restoration of Rod and Cone Vision by Single Dose rAAV-Mediated Gene Transfer to the Retina in a Canine Model of Childhood Blindness. Mol Ther. 2005; 12:1072–82. [PubMed: 16226919]
20. Allocca M, Doria M, Petrillo M, Colella P, Garcia-Hoyos M, Gibbs D, et al. Serotype-dependent packaging of large genes in adeno-associated viral vectors results in effective gene delivery in mice. J Clin Invest. 2008; 118:1955–64. [PubMed: 18414684]
21. Dong B, Nakai H, Xiao W. Characterization of genome integrity for oversized recombinant AAV vector. Mol Ther. 2010; 18:87–92. [PubMed: 19904236]
22. Lai Y, Yue Y, Duan D. Evidence for the failure of adeno-associated virus serotyp. 5 to package a viral genome > 8.2 kb. Mol Ther. 2010; 18:75–9. [PubMed: 19904238]
23. Wu Z, Yang H, Colosi P. Effect of genome size on AAV vector packaging. Mol Ther. 2010; 18:80–6. [PubMed: 19904234]
24. Odom GL, Gregorevic P, Allen JM, Chamberlain JS. Gene therapy of mdx mice with large truncated dystrophins generated by recombination using rAAV6. Molecular therapy : the journal of the American Society of Gene Therapy. 2011; 19:36–45. [PubMed: 20859263]
25. Zhang Y, Duan D. Novel mini-dystrophin gene dual adeno-associated virus vectors restore neuronal nitric oxide synthase expression at the sarcolemma. Human gene therapy. 2012; 23:98–103. [PubMed: 21933029]
26. Haire SE, Pang J, Boye SL, Sokal I, Craft CM, Palczewski K, et al. Light-driven cone arrestin translocation in cones of postnatal guanylate cyclase-1 knockout mouse retina treated with AAV-GC1. Investigative ophthalmology & visual science. 2006; 47:3745–53. [PubMed: 16936082]

27. Pang JJ, Lauramore A, Deng WT, Li Q, Doyle TJ, Chiodo V, et al. Comparative analysis of in vivo and in vitro AAV vector transduction in the neonatal mouse retina: effects of serotype and site of administration. Vision research. 2008; 48:377–85. [PubMed: 17950399]

28. Hasson T, Heintzelman MB, Santos-Sacchi J, Corey DP, Mooseker MS. Expression in cochlea and retina of myosin VIIa, the gene product defective in Usher syndrome type 1B. Proc Natl Acad Sci USA. 1995; 92:9815–9819. [PubMed: 7568224]

29. Liu X, Vansant G, Udovichenko IP, Wolfrum U, Williams DS. Myosin VIIa, the product of the Usher 1B syndrome gene, is concentrated in the connecting cilia of photoreceptor cells. Cell Motil Cytoskel. 1997; 37:240–252.

30. Williams DS. Usher syndrome: Animal models, retinal function of Usher proteins, and prospects for gene therapy. Vision Res. 2008; 48:433–41. [PubMed: 17936325]

31. Klomp AE, Teofilo K, Legacki E, Williams DS. Analysis of the linkage of MYRIP and MYO7A to melanosomes by RAB27A in retinal pigment epithelial cells. Cell Motil Cytoskeleton. 2007; 64:474–87. [PubMed: 17352418]

32. Lopes VS, Ramalho JS, Owen DM, Karl MO, Strauss O, Futter CE, et al. The ternary Rab27a-Myrip-Myosin VIIa complex regulates melanosome motility in the retinal pigment epithelium. Traffic. 2007; 8:486–99. [PubMed: 17451552]

33. Bostick B, Shin JH, Yue Y, Duan D. AAV-microdystrophin therapy improves cardiac performance in aged female mdx mice. Molecular therapy : the journal of the American Society of Gene Therapy. 2011; 19:1826–32. [PubMed: 21811246]

34. Schwander M, Lopes V, Sczaniecka A, Gibbs D, Lillo C, Delano D, et al. A novel allele of myosin VIIa reveals a critical function for the C-terminal FERM domain for melanosome transport in retinal pigment epithelial cells. J Neurosci. 2009; 29:15810–8. [PubMed: 20016096]

35. Yang Y, Baboolal TG, Siththanandan V, Chen M, Walker ML, Knight PJ, et al. A FERM domain autoregulates Drosophila myosin 7a activity. Proc Natl Acad Sci U S A. 2009; 106:4189–94. [PubMed: 19255446]

36. Wu L, Pan L, Wei Z, Zhang M. Structure of MyTH4-FERM domains in myosin VIIa tail bound to cargo. Science. 2011; 331:757–60. [PubMed: 21311020]

37. Kapranov P, Chen L, Dederich D, Dong B, He J, Steinmann KE, et al. Native molecular state of adeno-associated viral vectors revealed by single-molecule sequencing. Human gene therapy. 2012; 23:46–55. [PubMed: 21875357]

38. Halbert CL, Allen JM, Miller AD. Efficient mouse airway transduction following recombination between AAV vectors carrying parts of a larger gene. Nature biotechnology. 2002; 20:697–701.

39. Ghosh A, Yue Y, Duan D. Viral serotype and the transgene sequence influence overlapping adeno-associated viral (AAV) vector-mediated gene transfer in skeletal muscle. The journal of gene medicine. 2006; 8:298–305. [PubMed: 16385549]

40. Duan D, Yue Y, Engelhardt JF. Expanding AAV packaging capacity with trans-splicing or overlapping vectors: a quantitative comparison. Molecular therapy : the journal of the American Society of Gene Therapy. 2001; 4:383–91. [PubMed: 11592843]

41. Ghosh A, Yue Y, Lai Y, Duan D. A hybrid vector system expands adeno-associated viral vector packaging capacity in a transgene-independent manner. Molecular therapy : the journal of the American Society of Gene Therapy. 2008; 16:124–30. [PubMed: 17984978]

42. Auricchio A, Kobinger G, Anand V, Hildinger M, O'Connor E, Maguire AM, et al. Exchange of surface proteins impacts on viral vector cellular specificity and transduction characteristics: the retina as a model. Human molecular genetics. 2001; 10:3075–81. [PubMed: 11751689]

43. Allocca M, Manfredi A, Iodice C, Di Vicino U, Auricchio A. AAV-mediated gene replacement, either alone or in combination with physical and pharmacological agents, results in partial and transient protection from photoreceptor degeneration associated with betaPDE deficiency. Investigative ophthalmology & visual science. 2011; 52:5713–9. [PubMed: 21273543]

44. Zhong L, Li B, Mah CS, Govindasamy L, Agbandje-McKenna M, Cooper M, et al. Next generation of adeno-associated viru. 2 vectors: point mutations in tyrosines lead to high-efficiency transduction at lower doses. Proceedings of the National Academy of Sciences of the United States of America. 2008; 105:7827–32. [PubMed: 18511559]

45. Boye SL, Conlon T, Erger K, Ryals R, Neeley A, Cossette T, et al. Long-term preservation of cone photoreceptors and restoration of cone function by gene therapy in the guanylate cyclase-1 knockout (GC1KO) mouse. Investigative ophthalmology & visual science. 2011; 52:7098–108. [PubMed: 21778276]

46. Pang JJ, Dai X, Boye SE, Barone I, Boye SL, Mao S, et al. Long-term retinal function and structure rescue using capsid mutant AAV8 vector in the rd10 mouse, a model of recessive retinitis pigmentosa. Molecular therapy : the journal of the American Society of Gene Therapy. 2011; 19:234–42. [PubMed: 21139570]

47. Hasson T, Walsh J, Cable J, Mooseker MS, Brown SDM, Steel KP. Effects of shaker. 1 mutations on myosin-VIIa protein and mRNA expression. Cell Motility and the Cytoskeleton. 1997; 37:127–138. [PubMed: 9186010]

48. Gibbs D, Diemer T, Khanobdee K, Hu J, Bok D, Williams DS. Function of MYO7A in the human RPE and the validity of shaker1 mice as a model for Usher syndrome 1B. Invest Ophthalmol Vis Sci. 2010; 51:1130–5. [PubMed: 19643958]

49. Gibson F, Walsh J, Mburu P, Varela A, Brown KA, Antonio M, et al. A type VII myosin encoded by mouse deafness gene shaker-1. Nature. 1995; 374:62–64. [PubMed: 7870172]

50. Zolotukhin S, Potter M, Zolotukhin I, Sakai Y, Loiler S, Fraites TJ Jr. et al. Production and purification of serotype 1, 2, an. 5 recombinant adeno-associated viral vectors. Methods. 2002; 28:158–67. [PubMed: 12413414]

51. Jacobson SG, Acland GM, Aguirre GD, Aleman TS, Schwartz SB, Cideciyan AV, et al. Safety of recombinant adeno-associated virus type 2-RPE65 vector delivered by ocular subretinal injection. Molecular therapy : the journal of the American Society of Gene Therapy. 2006; 13:1074–84. [PubMed: 16644289]

52. Gibbs D, Williams DS. Isolation and culture of primary mouse retinal pigmented epithlelial cells. Adv Exp Med Biol. 2003; 533:347–352. [PubMed: 15180284]

53. Soni LE, Warren CM, Bucci C, Orten DJ, Hasson T. The unconventional myosin-VIIa associates with lysosomes. Cell Motil Cytoskeleton. 2005; 62:13–26. [PubMed: 16001398]

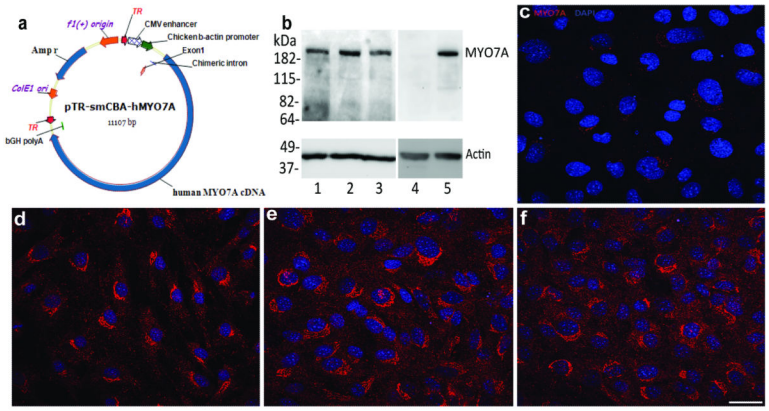

Fig. 1.

Expression of MYO7A from single AAV2 and AAV5 vectors in cultured cells. (**a**) Diagram of the viral vector encoding human *MYO7A* cDNA. (**b**) Western blot of WT eyecup (lane 1), primary RPE cultures derived from *Myo7a*-null mice and infected with AAV2-*MYO7A* (lane 2) or AAV5-*MYO7A* (lane 3), or not infected (lane 4), and primary RPE cultures derived from *Myo7a*$^{+/-}$ mice (lane 5). All lanes were immunolabeled with antibodies against actin (as a loading indicator of relative protein loading) and MYO7A. (**c-f**) Immunofluorescence images of primary RPE cell cultures. Cells derived from *Myo7a*-null mice that were not infected (c), from *Myo7a*$^{+/-}$ mice (d), or from *Myo7a*-null mice infected with 1x AAV2-MYO7A (e) or 1x AAV5-MYO7A (f). Scale = 10 μm.

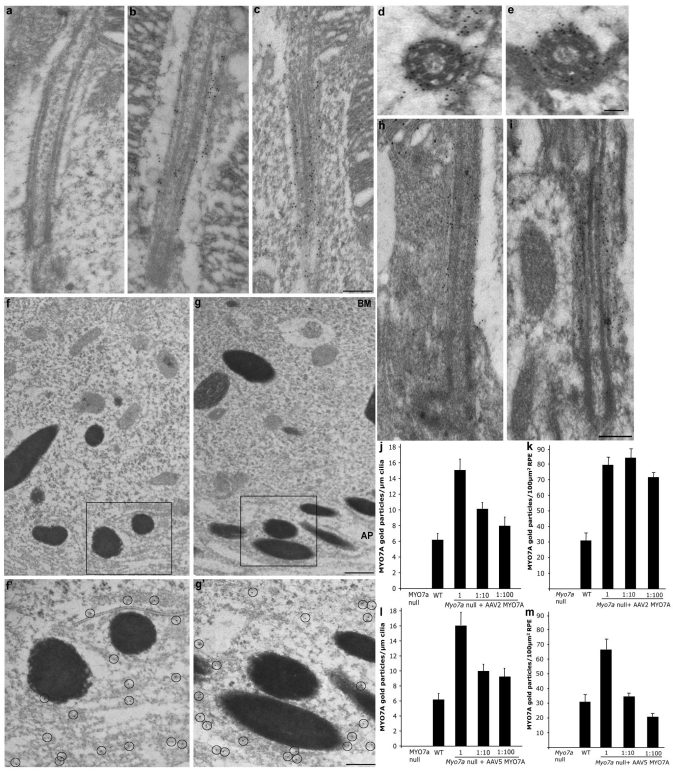

Fig. 2.

Expression of MYO7A from single AAV2 and AAV5 vectors *in vivo*. (**a-e**) EM images of MYO7A immunogold labelling of the connecting cilium and pericilium from rod photoreceptors in a *Myo7a*-null retina. (**a**) Longitudinal section from an untreated *Myo7a*-null retina (background label only). (**b, c**) Longitudinal sections from *Myo7a*-null retinas treated with 1x AAV2-*MYO7A* (**b**) or AAV5-*MYO7A* (**c**). Scale = 200 nm. (**d, e**) Transverse sections of connecting cilia from rod photoreceptors in *Myo7a*-null retinas treated with 1x AAV2-*MYO7A* (**d**) or AAV5-*MYO7A* (**e**). Scale = 100 nm. (**f-g**) EM images of RPE cells from *Myo7a*-null retinas treated with 1x AAV2-*MYO7A* (**f**) or AAV5-*MYO7A* (**g**). Scale = 2 μm. BM = Bruch's Membrane, AP = Apical Processes. Areas indicated by rectangles are enlarged in f' and g', in order to show MYO7A immunogold labeling (indicated by circles). Scale = 500 nm. (**h, i**) EM image of a longitudinal section of the connecting cilium and pericilium from a rod (h) and a cone (i) photoreceptor in a *Myo7a*-null retina, treated with 1x AAV2-*MYO7A*. The section was double-labeled with MYO7A (12 nm gold) and rod opsin (15 nm gold) antibodies. Rod outer segments were labeled with the opsin antibody, while cones were identified by lack of rod opsin labeling in their outer segments. The sections show just the base of the outer segments. Nearly all the label in the connecting cilium is MYO7A, even in the rod. Scale = 200 nm. (**i-l**) Bar graphs indicating MYO7A immunogold particle density in the rod photoreceptor cilium and pericilium (**j, k**) and in the RPE (**l, m**), following treatment with AAV2-*MYO7A* (**j, l**) or AAV5-*MYO7A* (**k, m**) of different concentrations. n=3 animals per condition. Bars indicate SEM.

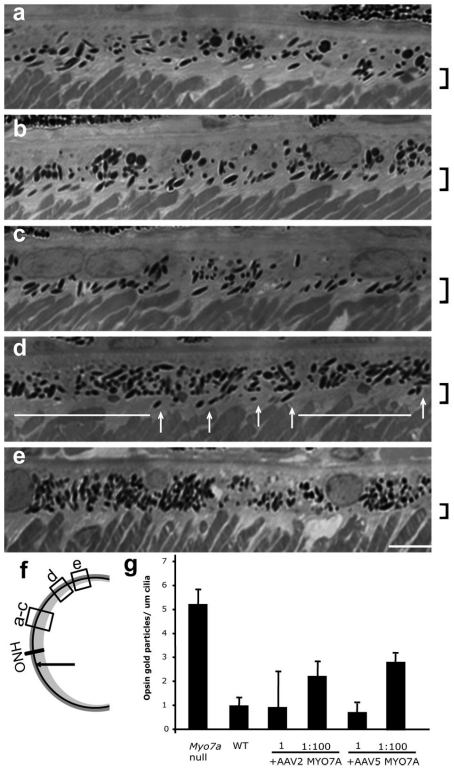

Fig. 3.

Correction of mutant phenotypes, following subretinal injections with AAV2-*MYO7A* or AAV5-*MYO7A*. (**a-e**) Correction of melanosome localization. Light micrographs showing the presence of melanosomes in the apical processes of the RPE in a WT retina (**a**) and retinas injected with 1x AAV2-*MYO7A* (**b**) or AAV5-*MYO7A* (**c**). Further away from the injection site (**d**), melanosomes are present in the apical processes of some RPE cells, but not in others (arrows indicate apical melanosomes; white lines indicate regions where melanosomes are absent from the apical processes). (**e**) Region distant from injection site, where all RPE cells lack melanosomes in their apical processes. Brackets on left side indicate RPE apical processes. Scale = 8 μm. (**f**) Diagram of a dorso-ventral section through an eyecup, indicating the relative locations of the images shown in a-e. Arrow indicates the site of injection, ONH indicates the optic nerve head. (**g**) Correction of abnormal levels of opsin in the connecting cilium and pericilium of rod photoreceptors. Bar graph showing opsin immunogold gold particle density, along the length of the connecting cilium. Ultrathin sections of retinas from *Myo7a*-null and WT mice were stained with rod opsin antibody. The *Myo7a*-null retinas had been either not treated or treated with 1x or 1:100 AAV2-*MYO7A* or AAV5-*MYO7A*. N = 3 animals per condition. Bars indicate SEM.

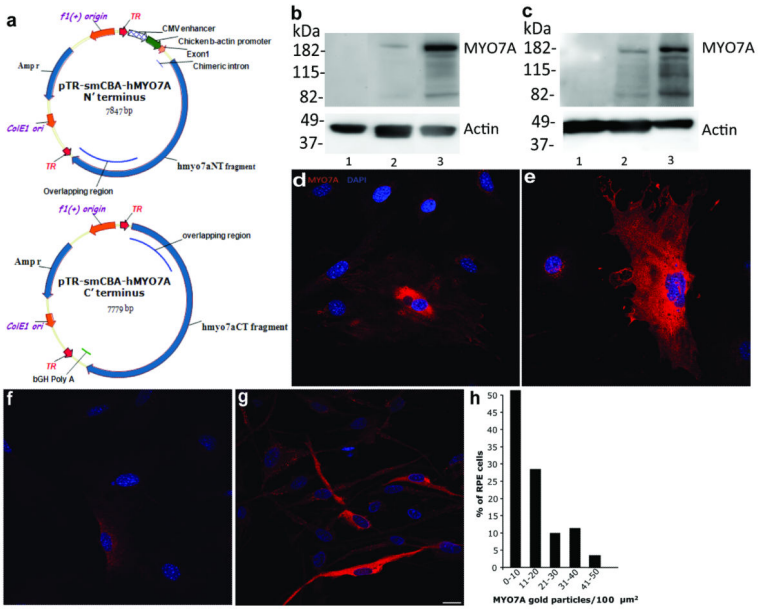

Fig. 4.

Expression of MYO7A from the overlapping AAV2-*MYO7A* dual vectors. (**a**) Diagram of the the overlapping AAV2-*MYO7A* dual vectors. The overlapping region contains 1365 bases. (**b**) Western blot of proteins from primary RPE cultures derived from *Myo7a*-null mice and not infected (lane 1), or infected with AAV2-*MYO7A*(dual) (lane 2); and primary RPE cultures derived from *Myo7a*$^{+/-}$ mice (lane 3). All lanes were immunolabeled with anti-MYO7A and anti-actin. (**c**) Western blot of primary cultures derived from *Myo7a*-null mice and not infected (lane 1), or infected with AAV2-*MYO7A*(dual (lane 2) or with AAV5-*MYO7A* single vector (1x) (lane 3). Lanes were immunolabeled with anti-MYO7A and anti-actin. Densitometry of the actin labeling showed that lane 2 was loaded with 3-fold more protein than lane 3; the MYO7A to actin ratio is 7-fold greater in lane 3 compared with lane 2 in this blot. (**d-g**) Immunofluorescence of cultured RPE cells transduced with AAV2-MYO7A(dual). (**d-f**) Primary RPE cultures derived from *Myo7a*-null mice and (**g**) ARPE19 cells. Scale = 10 µm. (**h**) Bar graph indicating the distribution of MYO7A immunogold particle density among RPE cells from retinas of *Myo7a*-null mice, injected with AAV2-MYO7A(dual). N = 3 animals.

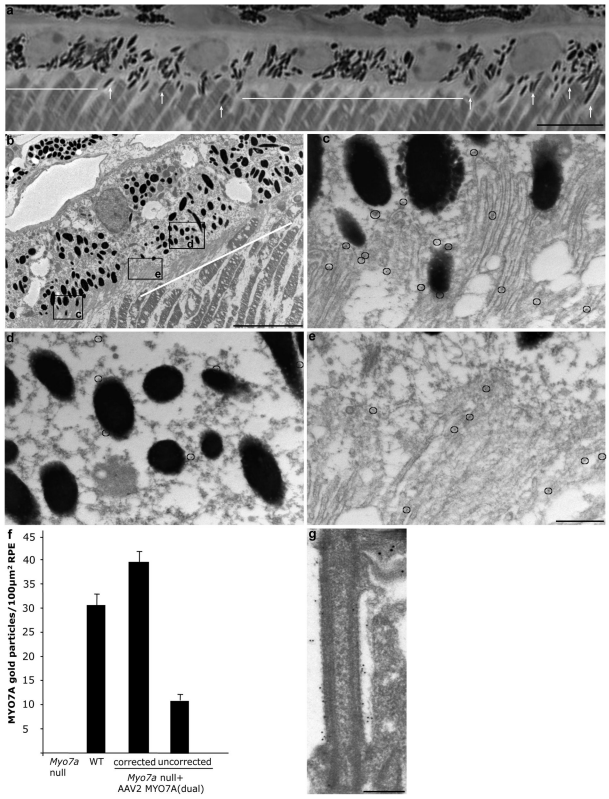

Fig. 5.

Correction of mutant phenotypes, following subretinal injections with AAV2-*MYO7A*(dual). (**a**) Light microscopy of a semi-thin section from a treated *Myo7a*-null mouse retina. Region shown is near the injection site. Arrows indicate melanosomes in the apical processes. White lines indicate cells that still show the *Myo7a*-null phenotype, with an absence of melanosomes in the apical processes. Scale = 10 μm. (**b**) Low magnification of an immunoEM image of the RPE from a retina treated with AAV2-*MYO7A*(dual). As in **a**, the white line indicates a region that still shows the *Myo7a*-null phenotype. Rectangle, c, includes melanosomes in the apical region, indicating a corrected RPE cell. Scale = 10 μm. (**c-e**) Higher magnification of regions outlined by rectangles in **b**. MYO7A immunogold particles are indicated by circles. Scale = 1 μm. (**f**) Bar graph illustrating MYO7A immunogold particle density measured in RPE cells from *Myo7a*-null retinas, WT retinas, or from *Myo7a*-null retinas treated with AAV2-*MYO7A*(dual) and determined to be corrected or not corrected by the location of their apical melanosomes. N = 3 animals per condition. Bars indicate SEM. (**g**) ImmunoEM image of a rod photoreceptor cilium double-labeled with antibodies against MYO7A (small gold particles) and against rod opsin (large gold particles). MYO7A labeling is associated with the connecting cilium and periciliary membrane, indicating expression and correct localization of MYO7A, while this region is devoid of opsin labeling, which is restricted to the disk membranes, consistent with the WT phenotype, thus indicating correction of the mutant phenotype. Scale = 300 nm.